Evaluation of Damage Fields Near Crack Tips in a Composite Solid Propellant

C. T. Liu*
Astronautics Laboratory (AFSC), Edwards Air Force Base, California 93523

The damage characteristics in precracked composite solid-propellant specimens subjected to a complex cyclic loading history are investigated using acoustic imaging techniques. The acoustic imaging data are analyzed to delineate the damage field ahead of the crack tips and to generate contour plots of the damage intensity. The results of these analyses are compared and the effect of loading history on damage characteristics is discussed.

Introduction

COMPOSITE solid propellants are filled elastometers containing solid particles. Therefore, it is expected that on the microscopic scale, a highly filled solid propellant can be considered a nonhomogeneous material. When this material is strained, the different size and the distribution of the filler particles, the variation of the bond strength between the particles and the binder, and the different crosslink density of polymer chains can all produce a highly nonhomogeneous local stress field. Also, this material may contain randomly spaced microids, incipient damage sites, and microcracks with statistically distributed sizes and directions. Therefore, the local strength in the material varies in a random fashion, so the failure sites in the material do not necessarily coincide with the maximum stress location. Hence, the failure location, as well as the degree of damage induced in the material will also vary in a random fashion. The damage developed in the material may be in the form of microcracks or microvoids in the binder or in the form of dewetting between the binder and the particle. The developed damage will not be confined to a specific location; rather, it will diffuse into a relatively large area or zone. The growth of the damage in the material may take place by the material tearing or by successive nucleation and coalescence of the microvoids. These cumulative damage processes are time-dependent and are the main factors responsible for the time-sensitivity of the strength degradation as well as the fracture of the material. Therefore, to gain an advanced understanding of the solid-propellant failure behavior, detailed knowledge of the damage characteristics is required.

In the past, acoustic imaging techniques were used to determine the damage field near the crack tips in solid propellants.[1-3] Experimental results indicated that damage occurred near the crack tip and, initially, the damage zone's shape was very similar to the plastic zone's shape near the crack tip in metals. However, when the strain level was increased, the damage zone's shape became irregular. Experimental results, obtained from cyclic tests, also revealed that damage zone size and intensity of damage were highly dependent on the cyclic loading history. In addition, a comparison of the results of the finite-element analysis with the results of acoustic imaging test reveals that the damage distribution is roughly commensurate with the strain distribution in the specimen, as shown in Refs. 2 and 3.

In this study, the characteristics of the damage field near the tips of the cracks in a composite solid propellant subjected to complex loading histories were investigated using sheet tensile specimens. The specimens' dimensions were 7.62 × 6.35 × 0.508 cm (3 × 2.5 × 0.2 in.). Two 2.54-cm (1.0 in.) cracks at the edges of the specimen were cut through the thickness of the specimen with a razor blade. Acoustic imaging test results were plotted in the form of iso-intensity contours of the transmitted acoustic energy to enhance resolution of the damage field. The results of these analyses were compared, and the effects of loading history on damage characteristics were evaluated. In addition to the experimental analysis, Texas Grain Analysis Program-2D (TEXGAP-2D), a finite-element computer code, was used to analyze the specimen under a constant strain condition. The strain distribution, obtained from the finite-element analysis, and the damage distribution, obtained from acoustic imaging tests, are compared and the results are discussed.

Specimen and Testing

The effect of cyclic loading on damage characteristics in a composite solid propellant was investigated using precracked specimen. The geometry of the precracked specimen containing two 2.54-cm (1.0 in.) cracks is shown in Fig. 1. The cyclic loading is schematically shown in Fig. 2.

In this study, the Lockheed Research Laboratory's acoustic-imaging system, shown in Fig. 3, was used to measure the attenuation difference in a scanning mode. Because acoustic imaging is conveniently performed in a water tank, a Lucite container was constructed to hold glycerol fluid in which a straining device could be immersed. This container was, in turn, immersed in a water tank. During the test, the acoustic wave of a wavelength short enough to exhibit quasioptical be-

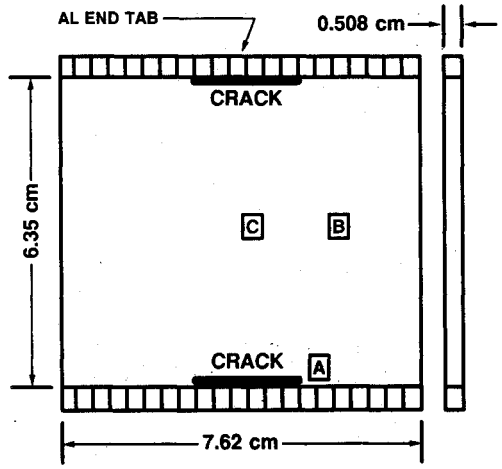

Fig. 1 Specimen geometry.

Presented as Paper 88-2284 at the AIAA/ASME/ASCE/AHS 29th Structures, Structural Dynamics, and Materials Conference, Williamsburg, VA, April 18-20, 1988; received Dec. 9, 1988; revision received May 13, 1990; accepted for publication May 25, 1990.

*Senior Research Engineer. Member AIAA.

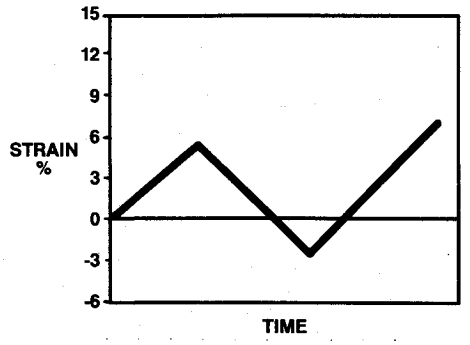

Fig. 2 Schematic representation of cyclic loading.

havior was radiated from an insonifier combined with a plane-concave polystyrene lens that focused acoustic energy at a desired location in the material to be studied. Acoustic energy passing through the material was recovered by a receiver lens of similar geometry and configuration, which transmitted the acoustic energy to a receiving transducer. The receiving transducer converted the transmitted acoustic energy into a corresponding electrical signal that was stored in a computer for further data analysis.

A two-dimensional acoustic image is generated in a common focal plane of the lenses by mechanical translation of the two lens/transducer units together in a plane normal to the acoustic transmission path. Each translation generates one scan line in the image. After each scan line has been completed, the scan mechanism steps one unit in evaluation, and another line scan is performed. Approximately 512 data points are generated per scan line, and 100 lines are scanned per inch of test material. An ultrasonic frequency of 1.9 MHz is used in the test. A detailed description of the testing setup and some of the basic components used in the acoustic imaging system can be found in Ref. 1.

The recorded experimental data were processed to create a visual indication of the energy absorbed in the material being inspected. A region of high ultrasonic absorption, i.e., a highly damaged area, will be shown as a dark area, and a region of unattenuated ultrasonic wave will produce a light or white area with 255 shades of grey in between. The acoustic image at a given strain level was plotted in the form of iso-intensity contours to enhance the resolution of the damage field. The results of these analyses are discussed in the following paragraphs.

Table 1 Results of finite-element stress analysis

	Specimen type	Crack length, cm	K_I, kPa, $cm^{1/2}$	K_{II}, kPa, $cm^{1/2}$
1	Edge crack	2.54	106.3	−14.7
	Center crack	3.81	178.3	6.4
2	Edge crack	2.54	207.5	5.9

Finite-Element Analysis

In this study, the stress field and the stress intensity factors at the tips of the crack in the specimen were determined using TEXGAP-2D finite-element computer code. The TEXGAP-2D computer code contains conventional crack elements derived from a hybrid displacement mode. These crack elements, originally developed by Kathireson and Alturi,[4] were used to calculate the stress intensity factors at the crack tips. In the analysis, a Poisson's ratio of 0.49999 and a modulus of 3448 kPa (500 psi) were used, and a constant displacement of 1.27 mm (0.05 in.) was applied to the top and bottom edges of the specimen. In this study, two types of cracked specimen were considered. One cracked specimen had two 2.54-cm (1.0 in.) cracks at the edges of the specimen and the other cracked specimen had one 3.81 cm (1.5 in.) crack at the center and two 2.54 (1.0 in.) cracks at the edge of the specimen. The finite-element model of the cracked specimen is shown in Fig. 4, along with iso-strain contours in the analyzed specimen with two edge cracks.

Results and Discussion

For the first type of cracked specimen analyzed, the results of the finite-element analyses indicated that the values of the mode I and mode II stress intensity factors K_I and K_{II} at the tip of the center crack are higher than that at the tips of the two edge cracks, as shown in Table 1. From Table 1, we note that the values of K_I and K_{II} at the tips of the two edge cracks in the second type of cracked specimen are higher than that in the first type of cracked specimen. This indicates that the

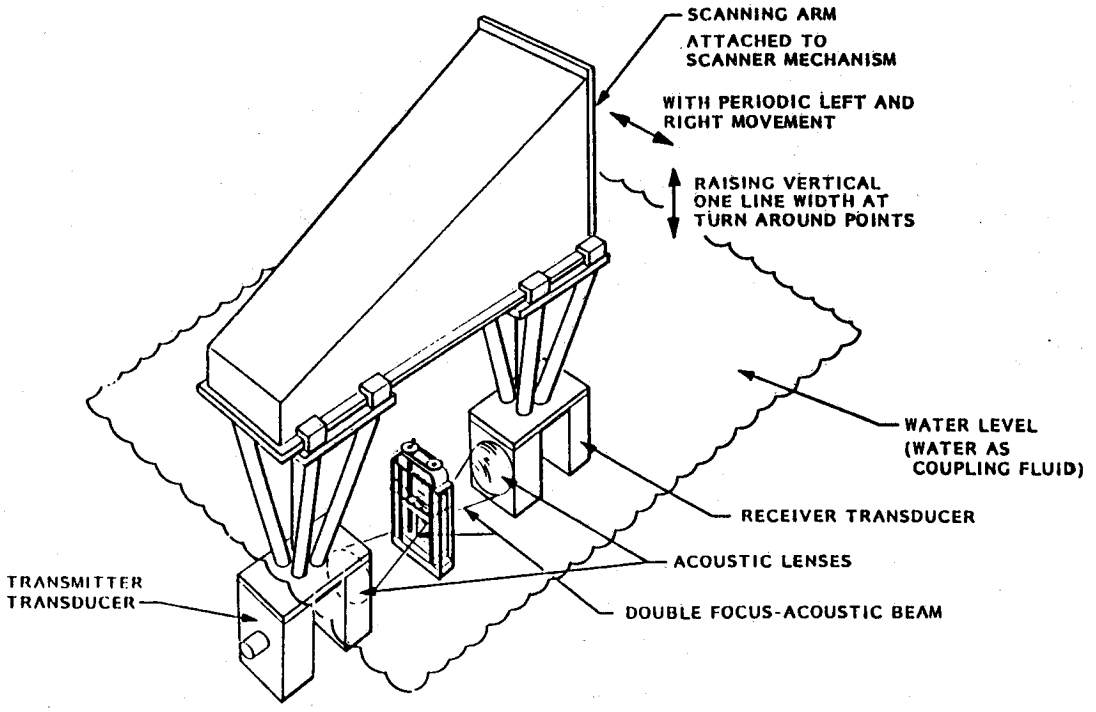

Fig. 3 Acoustic imaging testing system.

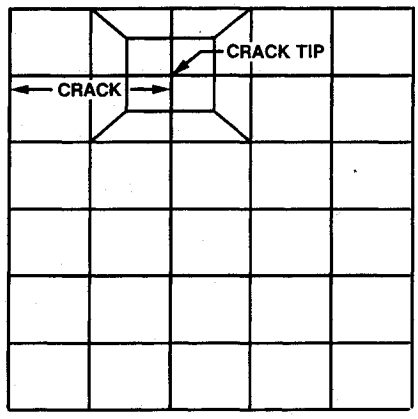

a) Finite-element model (¼ of the specimen)

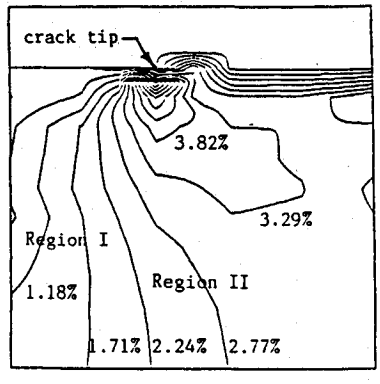

b) Iso-strain contours

Fig. 4 Finite-element model and iso-strain contours of maximum principal strain.

relatively longer center crack produces a "shielding" effect on the two edge cracks. In addition to the calculation of the stress intensity factors, the maximum principal stress and the maximum principal strain were also calculated, and iso-strain contours were plotted, as shown in Fig. 4. In Fig. 4, it is seen that the magnitude of the principal strain between the two edge cracks in the center region is small, compared with the strain in the region between the vertical edge of the specimen and an approximately vertical line drawn through the two crack tips. In the text, the low-stress strain region and the high strain region are denoted as region I and region II, respectively. It should be pointed out that the TEXGAP-2D computer code is an elastic finite-element computer code and, therefore, the calculated strains are elastic strains. It is known that the elastic strains are not accurate to describe the strain distributions in the crack-tip region because of the occurrence of a large deformation at the crack tip. Since the applied strain is low, the size of the highly deformed region is small. Consequently, the calculated elastic strains in the regions considered for the acoustic attenuation measurements should be reasonably accurate; therefore, it is used to explain the results of the acoustic imaging tests described in the following.

By examining the acoustic image of the virgin solid propellant specimen, the most prominent feature of the virgin specimen's acoustic image revealed is its dappled appearance. The dappled appearance may be due to a number of reasons, such as the existence of a cluster of filler particles in a small region, undercure of binder material in a local area, or large voids in the material. This dappled appearance is also an indication of the material's nonhomogeneity. When the specimen is strained, the high intensity of stress near the crack tip will induce a higher damage in the material. As the material is damaged, the acoustic energy transmitted through the damaged region will be attenuated or the intensity of the transmitted energy I_t will be decreased, resulting in a dark area near the crack tip. The size of the dark area or the size of the damage area increases with increasing strain level. In order to delineate the damage zone and the intensity of damage in the damage zone, the acoustic imaging data were analyzed and contours of iso-intensity of I_t were plotted. The results are discussed in the following paragraphs.

Plots of iso-intensity contours of I_t as a function of the applied global strain are shown in Fig. 5. In Fig. 5, the number between two contour lines is the range of I_t between the prior and the next intensity levels. The small number indicates that the intensity of the transmitted acoustic energy is low, or the damage level is high. These contour plots reveal that the size of the damage zone and the intensity of damage in the damage zone increases as the strain level is increased. According to Fig. 5b, the degree of damage in the center of the specimen, or region I, is relatively low, and the shape of the iso-intensity contours of I_t, or the shape of the damage zones, is similar to the iso-strain contours shown in Fig. 4. This implies that the damage distribution is roughly commensurate with the strain distribution in the specimen. It is interesting to note that the increase in strain from 3 to 6% produces a negligible effect on the damage intensity and damage zone size in the center region of the specimen. It should be pointed out that, because of acoustic noise, the size of the apparent crack, as shown in Fig. 5, is relatively larger than the actual crack.

When the specimen is unloaded from 6 to 0%, the experimental results, shown in Figs. 5d and 5e, reveal that the damage zone size and the intensity of damage decrease as the applied strain is reduced. A comparison of Fig. 5a with Fig. 5e shows that extensive damage developed near the crack tip region during the first strain cycle; the existence of the damaged regions indicates that, although the applied strain is zero at the end of the first strain cycle, the local microstrain is not zero. The existence of tensile residual strain will prevent the microvoids and microcracks, generated by the previously applied strains, from closing in spite of the existence of a compressive residual stress field at the crack tip region. Experimental findings reported by Ronay[5] reveal that, after the applied strain was released, both longitudinal and transverse residual strains were developed near a circular cutout on the surface of a specimen made of an inert solid propellant. It was found that a relatively small longitudinal tensile residual strain and a relatively large transverse compressive residual strain developed near the edge of the circular cutout. The existence of the residual strain ahead of the crack tip is one of the reasons why the damage zone still exists when the specimen is unloaded to 0% strain. However, due to the material's viscoelastic nature and to the redistribution of the residual stress and the residual strain, the magnitudes of the residual stress and the residual strain will decrease as the length of time is increased, resulting in a continuous decrease of the microvoids and microcrack sizes. Consequently, the damage zone size, as well as the damage intensity, will decrease accordingly. This time-dependence of the damage characteristics, measured by the acoustic imaging technique, was reported in Ref. 2.

At the end of the first strain cycle, a -3% strain, or a compressive strain of 3%, was applied to the specimen, and the acoustic data are shown in Fig. 6. A comparison of Fig. 6 with Fig. 5e reveals that the size of the highly damaged regions near the crack tips is reduced and the size of the less damaged regions is increased. This phenomenon is believed to be due to the reduction of the sizes of the microdefects as a result of the presence of the compressive strain. After the specimen was imaged at -3% strain, it was unloaded to 0% strain and reloaded again according to the applied strain history shown in Fig. 2. The results of the acoustic imaging data are shown in Fig. 7. A comparison between Figs. 6 and 7a indicates that when the specimen is unloaded from -3% strain to 0% strain, the size of the highly damaged regions near the crack tip are further decreased and the size of the less damaged regions in the specimen are relatively unchanged. This phenome-

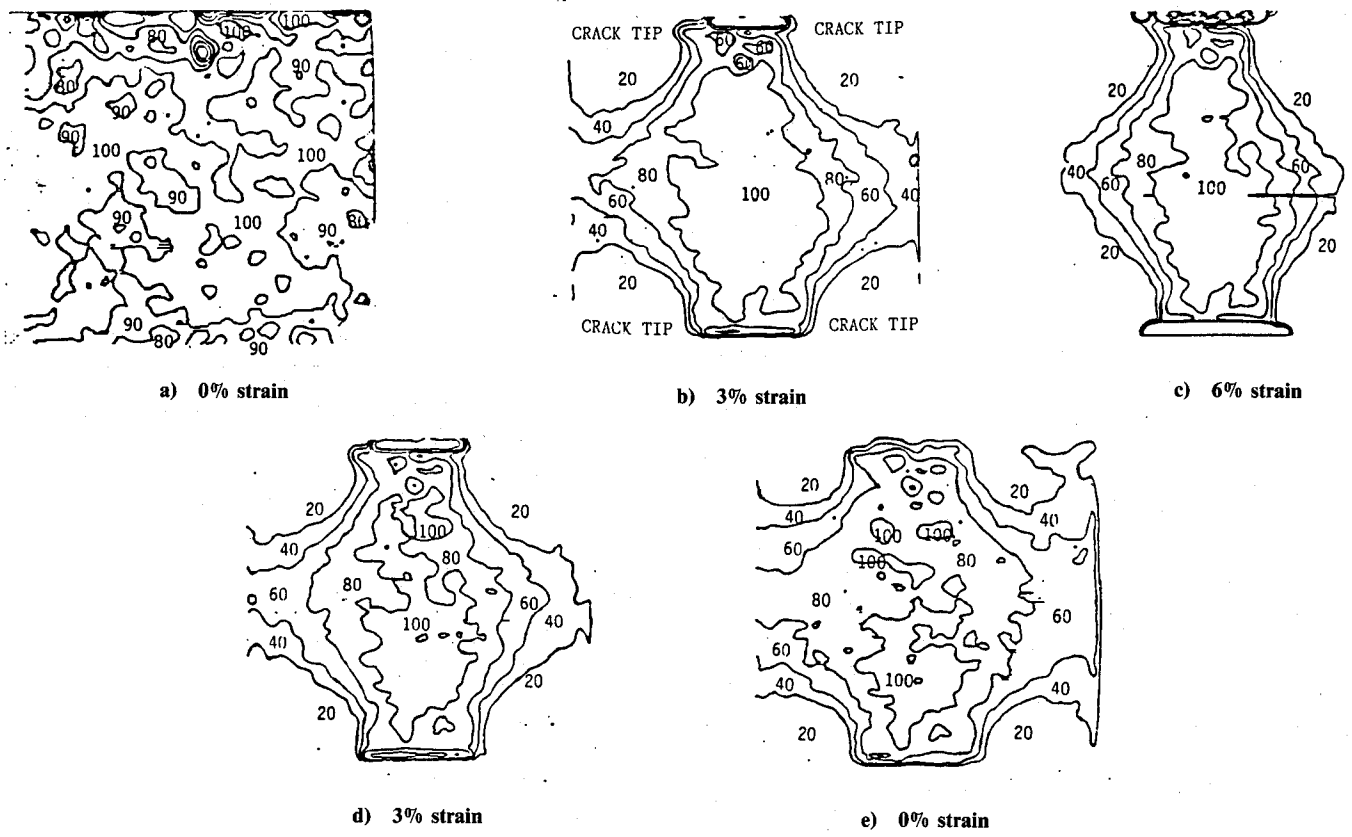

a) 0% strain b) 3% strain c) 6% strain

d) 3% strain e) 0% strain

Fig. 5 Iso-intensity contour plots of acoustic images of the propellant specimen (first strain cycle).

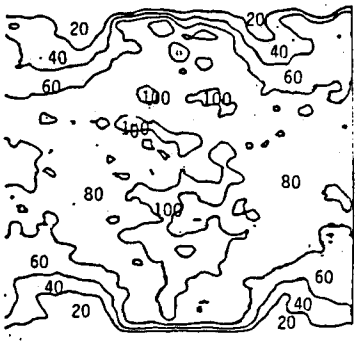

Fig. 6 Iso-intensity contour plot of acoustic image of the propellant specimen at −3% strain.

non is probably due to the material's viscoelastic nature and the rearrangement of material's microstructures in the high-stress regions near the crack tips. For a highly filled composite solid propellant, when the applied stress is reduced, the local compressive stresses between the filler particles may still be high enough to cause damage reduction and/or to decrease the size of existing microdefects, resulting in a decrease in the attenuation of acoustic energy. In addition, due to the material's viscoelastic nature, the local time-dependent material response may lag behind or may not be in phase with the applied load. The existence of time-scale or phase change between the applied load and the local material response is another possible contributing factor responsible for the decrease in damage zone size when the specimen is unloaded from −3% strain to 0% strain.

It is interesting to note that when the specimen is restrained after it is subjected to the compressive strain, the size of the highly damaged regions near the crack tips is smaller than that measured during the unloading branch of the first strain cycle. This indicates that the damage characteristics have been changed by the compressive strain. This experimental finding reveals that the material has a nonfading memory. In other words, the material remembers what happened to it before or remembers the past load history. Therefore, caution should be exercised when interpreting the acoustic imaging results or other nondestructive testing results to determine the damage state in solid propellants.

After the specimen was restrained to 6%, it was imaged and a 3.81 cm (1.5 in.) crack was cut at the center of the specimen while the specimen was held at 6% strain. The specimen was imaged immediately after the center crack was cut and also imaged at the subsequent strain levels with a 3% strain increment. The results of the acoustic imaging tests are shown in Figs. 7d and 7e. Figures 7c and 7d reveal that the presence of the center crack changes the values of I_t and the shapes of the iso-intensity contours of I_t near the tips of the center crack. However, the value of I_t and the shapes of the iso-intensity contours of I_t near the tips of the edge cracks are relatively unchanged.

By examining the specimen at 6% strain level, it was found that the center crack opened wider than the two edge cracks, or the crack opening displacement of the center crack was larger than that of the two edge cracks. It was also found that the crack opening displacement of the edge crack after the center crack was cut was smaller than that before the center crack was cut. When the strain level was increased to 9%, the crack opening displacements of the center and the edge cracks were increased, and the crack opening displacement of the center crack was still larger than that of the two edge cracks. This kind of experimental finding has not been observed when the center crack length is equal or shorter than the edge crack length, as shown in Ref. 3. In Ref. 3, after a precracked specimen was damaged by applying a cyclic strain load to it, a 1-in. crack, which was equal to the length of the top and the bottom cracks, was cut at the center specimen while the specimen was held at 3% strain. Experimental data revealed that the center crack did not open at this strain level, and it opened slightly

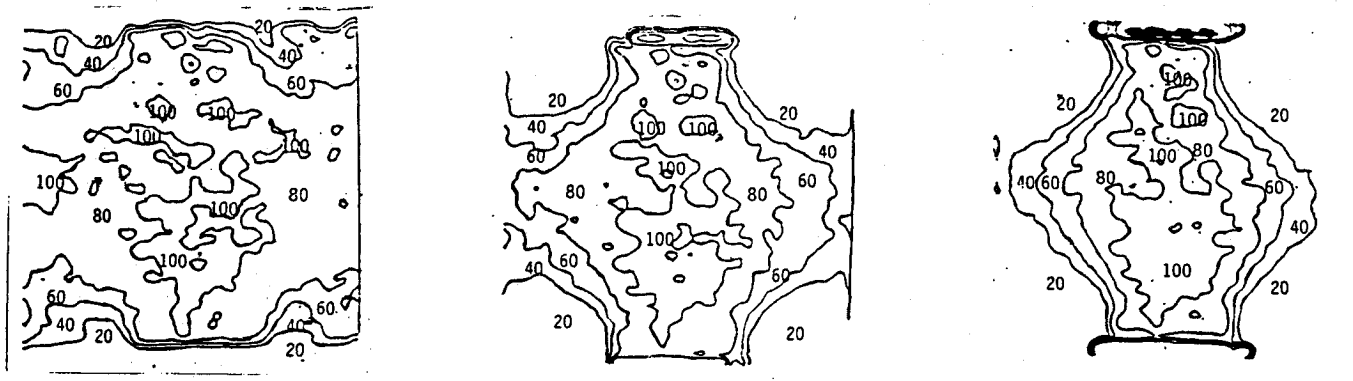

a) 0% strain b) 3% strain c) 6% strain, before the center crack was cut

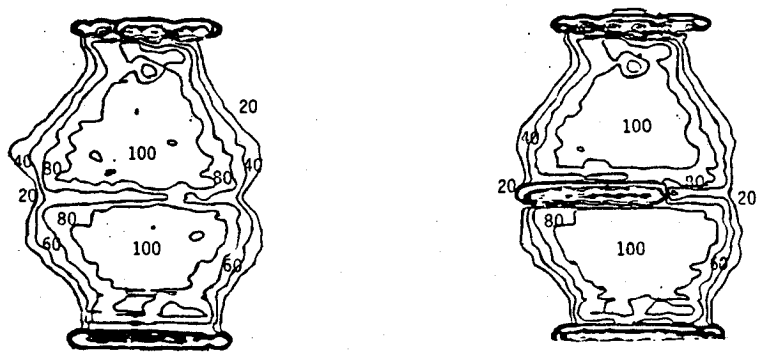

d) 6% strain, after the center crack was cut e) 9% strain

Fig. 7 Iso-intensity contour plots of acoustic images of the propellant specimen (second-strain cycle).

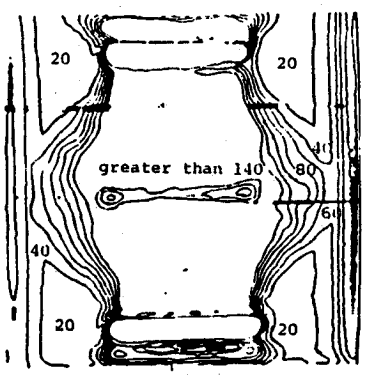

Fig. 8 Iso-intensity contour plot of acoustic image of the propellant specimen at 6% strain (center crack length equal to 1.0 in. and Fig. 12 in Ref. 3).

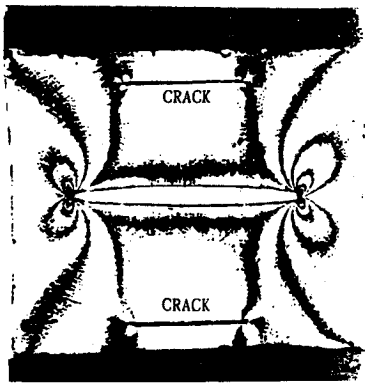

Fig. 9 Iso-chromatic fringe patterns for the photoelastic specimen at 6% strain.

when the strain was increased to 6%. As the strain was increased to 9%, the crack opening displacement of the center crack remained small and that of the other two cracks became relatively large. These experimental findings contradict the results of the finite-element stress analysis and the photoelastic test reported in Ref. 3. The results of the finite-element stress analysis and the photoelastic analysis indicated that the stress at the center crack opened relatively wider than the other two cracks. The results of photoelastic tests also indicated that the crack opening displacement of the center crack was independent of when the center crack was cut or whether it was cut before or after a cyclic load was applied to the specimen. These analytical and experimental findings, based on linear analyses, are not consistent with the experimental results reported in Ref. 3. The dependence of the crack opening displacement of the center crack on whether the specimen is prestrained or not is believed to be related to the microscopic damage generated in the material by prestraining, as discussed below.

It is well known that, for a given loading condition, the mechanical response and failure of composite solid propellants are closely related to the damage state in the material. Damage may be in the form of microvoids and/or microcracks in the binder, or in the form of the binder/particle separation known as dewetting. When the damage state reaches a critical value, the rigidity of the material is thereby reduced. Usually this critical dewetting state coincides with the transition from linear response to nonlinear behavior of composite solid propellants. Because of the nonhomogeneous nature of composite solid propellants, the generated microdefects will be distributed more or less randomly in the material. In addition, the orientation of these microdefects is also random with respect to the applied load. When this damaged material is stretched, these microdefects are oriented and the forces are

transmitted by a circuitous path passing between microdefects. Under this condition, the fracture path tends to straighten. This kind of material response is described by Smith et al.[6] as the geometrically nonlinear behavior at the microcrack level. Based on this discussion, it is believed that when the precracked specimen with two cracks is stretched, a large number of microdefects will be generated in the high-stress region (region II), and the stress in region II tends to straighten the fracture path or tends to rotate the microdefects toward the direction of the applied load. Consequently, a load path that transfers the applied load from one end of the specimen to the other is developed in the high-damage region (region II). The development of the load path is manifested by the iso-intensity contours of I_t in the high-stress region, as shown in Fig. 7c.

When a crack is cut at the center of the crack after the load path is developed, the opening of the center crack will be small if the center crack tips remain in the low-stress region. Based on this discussion, it is believed that the existence of the top and the bottom cracks, as well as the generation of damage in the high-stress regions, produces a "shielding" effect on the material in the center region of the specimen and on the center crack after it is cut. The degree of the shielding effect depends on the relative lengths of the center crack and the two edge cracks. When the length of center crack is equal or shorter than that of the top and the bottom cracks, the shielding effect is significant, as shown in Ref. 3 and in Fig. 8. On the other hand, when the length of the center crack is long enough and the crack tips are in the high-stress region, the shielding effect becomes less, as shown in Fig. 7d. It is interesting to point out that, for a linear material, when the center crack length is longer than the edge crack length, the center crack develops a significant shielding effect on the edge cracks, as shown in Fig. 9. However, for a nonlinear material, such as solid propellants with extensive damage developed in the material by previous loading, the shielding effect on the edge cracks becomes small, as shown in Figs. 7d and 7e. According to Figs. 7d and 7e, the presence of the center crack has a negligible effect on the damage characteristics near the tip of the bottom crack.

In this study, in addition to investigating the effect of cyclic loading on the damage field in the specimen, statistical analyses of I_t in a small area at three different locations were conducted. The small area had a dimension of 2.54 mm (0.1 in.) by 2.54 mm (0.1 in.), and it was located at three different places, denoted as A, B, and C (Fig. 1). In the statistical analyses, the mean and the standard deviation of I_t were calculated, and the histograms of I_t were plotted. The results of the statistical analyses are discussed below.

The mean value of I_t, or $\bar{I}_t$, in the small area near the right-side tip of the bottom crack (location A) was plotted as a function of the applied strain, and is shown in Fig. 10. From Fig. 10, we note that the value of $\bar{I}_t$ decreases as the strain level is increased. On the other hand, when the specimen is unloaded from 6% strain, the value of $\bar{I}_t$ increases with decreasing the strain level. In other words, the cyclic loading produces cyclic

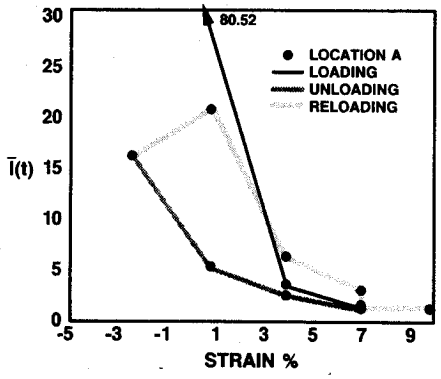

Fig. 10 Mean value of I_t vs applied strain (location A).

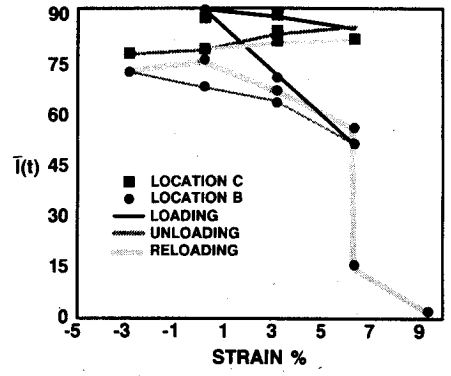

Fig. 11 Mean value of I_t vs applied strain (locations B and C).

behavior of $\bar{I}_t$. It is also noted that the $\bar{I}_t$ vs strain curve during the unloading branch of the cyclic loading is below the $\bar{I}_t$ vs strain curve during the loading branch of the cyclic loading. When the strain is reduced to 0% at the end of the first strain cycle, the value of $\bar{I}_t$ is much smaller than that of the virgin specimen, indicating the effect of the first strain cycle on the damage state in the specimen. When the specimen is compressed to 3% strain, the value of $\bar{I}_t$ at -3% is larger than that at 0% strain. This indicates that, under a compressive strain, the size of the microdefects are reduced, resulting in an increase in the value of $\bar{I}_t$. It is interesting to point out that when the specimen is unloaded from -3% strain to 0% strain, the value of $\bar{I}_t$ is increased from 16.75 to 21.38. This is probably because the local compressive stresses may still be high enough to decrease the size of the microdefects and the viscoelastic nature of the material, as discussed earlier. Referring to Fig. 10, when the specimen is reloaded from 0% strain after it is subjected to a -3% strain, the values of $\bar{I}_t$ calculated at the successive strain levels are larger than those calculated at the corresponding strain levels of the first strain cycle, indicating the effect of compressive strain on the damage state in the material measured at the subsequent strain levels.

Plots of $\bar{I}_t$ vs strain for locations B and C are shown in Fig. 11. According to Fig. 11, the curves of $\bar{I}_t$ for locations B and C, before the center crack is cut, show a similar cyclic behavior, except that the relative magnitudes of the value of $\bar{I}_t$ at 6% strain and at the subsequent strain levels during unloading are different for the two different locations. For location B, the value of $\bar{I}_t$ calculated at 3% and 0% during unloading are larger than that calculated at 6% strain, and the converse is true for location C. This phenomenon is believed to be due to the different strain distributions at the two locations. Based on the results of the finite-element stress analysis, the strain distribution at location B has not only a large gradient but also a large magnitude, whereas the strain distribution at location C is relatively uniform. For a relatively uniform strain distribution, the material in the small area may follow the same unloading stress-strain curve and may have the same retraction rate of microdefect size when the specimen is unloaded from 6% strain. On the other hand, for a nonuniform strain distribution, the material in the small area may follow different unloading stress-strain curves that, depending upon the magnitude of the maximum strain prior to unloading, may have different retraction rates of microdefect size when the specimen is unloaded from 6% strain. The dependence of unloading stress-strain curve and unloading retraction rate of microdefect size on the maximum strain level prior to unloading has been reported by Liu.[7] It was found that a higher maximum strain level prior to unloading produces a higher retraction rate of microdefect size. Consequently, when the specimen is unloaded, the highly damaged region in the high-strain area has a tendency to reduce its size at a higher rate, due to a higher rate of microdefect size reduction, as shown in Fig. 5. Under this condition, the nonuniform retraction rates of damage regions in the nonuniform strain field

may be a contributing factor responsible for the different phenomenon observed at locations B and C when the specimen is unloaded from 6% strain.

Conclusions

The effect of load history on the damage characteristics in a composite solid propellant has been investigated using acoustic imaging techniques. Experimental data indicate that the damage zone size and the damage intensity are dependent on the applied cyclic loading history and the induced local strain distribution. A comparison of the results of the finite-element stress analysis with the results of acoustic imaging tests reveals that the damage distribution is roughly commensurate with the strain distribution in the specimen. The experimental data also indicate that the degree of the shielding effect depends on the relative length of the center and the edge cracks as well as on the damage state in the specimen. In addition, the acoustic imaging data reveal that the current damage state depends on past loading history. Therefore, caution should be exercised when interpreting the acoustic imaging results or other nondestructive testing results to determine the damage state in solid propellants.

Acknowledgments

This work was supported by the Air Force Office of Scientific Research. The author would like to express his appreciation to R. Leighton for conducting the finite-element stress analysis, and to R. Yee of the Lockheed Research Laboratory for conducting the acousting imaging tests.

References

[1]Martinson, R. H., and Hartog, J. J., "Acoustic Imaging Applied to Crack Propagation Studies," JANNAF Structure and Mechanical Behavior Subcommittee 16th Meeting, CPIA Publication 311, Chemical Propulsion Information Agency, Laurel, MD, March 1980.

[2]Liu, C. T., and Yee, R., "Evaluation of Cumulative Damage in a Composite Solid Propellant," *Proceedings of the 1986 Society for Experimental Mechanics Conf. on Experimental Mechanics,* New Orleans, LA, June 8–13, 1986, pp. 729–736.

[3]Liu, C. T., "Investigating the Damage Field Near Crack Tips in a Composite Solid Propellant," *Proceedings of the 1987 Society for Experimental Mechanics Conf. on Experimental Mechanics,* Houston, TX, June 1987, pp. 453–461.

[4]Kathireson, K., and Alturi, S. N., "Three-Dimensional Homogeneous and Bi-Material Fracture Analysis for Solid Motor Grains by a Hybrid Displacement Finite Element Method," Air Force Rocket Propulsion Lab., AFRPL-TR-78-65, Georgia Inst. of Technology, Atlanta, GA, 1978.

[5]Ronay, M., "Non-Homogeneous Straining and Fracture Mechanism in a Filled Elastomer," Dept. of Civil Engineering and Engineering Mechanics, Columbia Univ., NY, TR No. 19, 1965.

[6]Smith, G. C., Palaniswamy, K., and Knauss, W. G., "The Application of Rate Theory to the Failure of Solid Propellants," Air Force Rocket Propulsion Lab., AFRPL-TR-73-54, Graduate Aeronautical Lab., California Inst. of Technology, Pasadena, CA, July 1973.

[7]Liu, C. T., "Effects of Cyclic Loading Sequence on Cumulative Damage and Constitutive Behavior of a Composite Solid Propellant," *Proceedings of the AIAA/ASME/ASCE/AHS 28th Structures, Structural Dynamics, and Materials Conf.,* AIAA, New York, April 1987.

David H. Allen
Associate Editor